JOURNAL OF THERMOPHYSICS AND HEAT TRANSFER
Vol. 12, No. 2, April–June 1998

Advanced Model of Nitric Oxide Formation in Hypersonic Flows

Deepak Bose* and Graham V. Candler†
University of Minnesota, Minneapolis, Minnesota 55455

A model for nitric oxide (NO) formation in low-density hypersonic flows is presented. The thermal nonequilibrium reaction rates, reactant energy removal rates, and product energy disposal rates are based on a quasiclassical trajectory analysis of the Zeldovich reactions. At hypersonic flow conditions, the newly obtained reaction rate for the second Zeldovich reaction is approximately an order of magnitude larger than the commonly used rate. The rate of this reaction is a weak function of the reactant internal energy, but it produces vibrationally excited NO molecules that result in an elevated NO vibrational temperature. A flowfield model that includes these effects is proposed, and a computational fluid dynamics method is used to simulate the BSUV1 and BSUV2 flight experiments. The new model generally improves the agreement with the spectrally resolved radiation data; however, it appears that there are additional mechanisms that preferentially remove the highly excited NO molecules.

Introduction

THE nitric oxide (NO) molecule is an important source of thermal radiation in hypersonic flows. Thus, accurate models for its formation rate and internal energy state are required. In hypersonic flows, NO is formed via the Zeldovich reactions

$$N_2 + O \rightarrow NO + N \quad (1)$$

$$O_2 + N \rightarrow NO + O \quad (2)$$

However, little is known about the kinetics of these reactions at the high temperatures that characterize hypersonic flows. Experimental investigations of these reactions are restricted to rate constant determinations at moderately high temperatures. The rates of reaction (1) are available up to 8000 K, and for reaction (2) up to 3000 K,[1] whereas the temperature in hypersonic flows may exceed 20,000 K. The reaction rates used for hypersonic flow calculations are obtained by extrapolating the low-temperature data, resulting in large uncertainties. In high-altitude hypersonic flows the gas is in a thermal nonequilibrium state, which affects the reaction rates; these nonequilibrium reaction rates are particularly difficult to obtain experimentally. It is also necessary to determine the internal energy state of the newly formed molecules, because these molecules require many collisions to vibrationally equilibrate. Therefore, the NO kinetics and radiative emission are strongly influenced by the molecules' nascent energy.

To adequately model these effects in flow simulation codes, a detailed theoretical study of reactions (1) and (2) is needed. We use a quasiclassical trajectory (QCT) method in which the classical equations of motion are used to simulate the molecular collisions on the relevant potential energy surfaces (PESs) obtained from ab initio computational chemistry studies.

Received Aug. 25, 1997; accepted for publication Nov. 24, 1997.

*Graduate Research Assistant, Department of Aerospace Engineering and Mechanics; currently Research Scientist, Thermosciences Institute, NASA Ames Research Center, Moffett Field, CA 94035. Member AIAA.

†Associate Professor, Department of Aerospace Engineering and Mechanics, Army High Performance Computing Research Center. Senior Member AIAA.

The authors carried out an extensive QCT study of reaction (1) to obtain various reaction attributes, such as the thermal rate constants, nonequilibrium rate constants, state-specific rate data, and product NO vibrational energy disposal.[2–4] Using the database obtained from this study, advanced models for this reaction were formulated. These models were obtained for both a continuum approach based on reactant temperatures[5] and for a particle simulation approach (DSMC) based on reactant collision energies.[6] Significant improvements in the kinetics of NO formation were obtained in high-altitude flows, which then explained the formation of vibrationally and rotationally hot NO observed in the BSUV flight experiments.[7,8]

A QCT study for reaction (2) has also been carried out by the authors.[9] The rate of this reaction is high because the reaction barrier is small. Thus, this reaction is likely to play an important role in flows where many N atoms are present. Also, past evidence indicates that this reaction produces vibrationally and rotationally hot NO molecules,[10,11] and the product energy disposal may be important for this reaction.

In this paper, we use the QCT database to develop a model for the formation of NO in high-temperature hypersonic flows. We include the effects of thermal nonequilibrium on the reaction rate and we model the vibrational and rotational energy of the newly formed NO molecules. We then use this model to simulate hypersonic flows over blunt bodies. It is found that although a detailed treatment of reaction (2) does not make a noticeable difference in the amount of NO produced, the vibrational energy disposal modeling makes significant differences in the vibrational temperature of NO in the flow regimes considered. The results of the simulations are used to compute uv spectral intensities from the NO bands. These are compared with the spectrometer data obtained from the flight experiments, and we find that the new models give improved agreement with the data.

Quasiclassical Trajectory Calculations

In Refs. 2 and 4, we studied reaction (1) using the two relevant potential energy surfaces (PESs) of the $3A''$ and $^3A'$ states, that join the reactants and the products in their ground electronic states

$$N_2(X\,^1\Sigma_g^+) + O(^3P) \rightarrow NO(X\,^2\Pi) + N(^4S)$$

The QCT data for reaction (2) with its reactants and products in their ground electronic states are presented in Ref. 9

$$O_2(X\,^3\Sigma_g^-) + N(^4S) \rightarrow NO(X\,^2\Pi) + O(^3P)$$

This reaction occurs on the two lowest PESs of the $^2A'$ and $^4A'$ states.[12,13] The ab initio studies of these surfaces were conducted by Walch and Jaffe,[13,14] and the analytical surface fits of Duff[11] are employed in the current study.

A quasiclassical trajectory code written in CMFORTRAN with a standard Monte Carlo[15] approach is used on the Thinking Machines Connection Machine-5 (CM-5). For each case, depending on its energy, between 16,384 and 131,072 trajectories are run. A fourth-order Runge–Kutta algorithm with a constant time step is used for the time integration. All trajectories are started by placing the N atom 9 Å away from the O_2 molecule and are finished when the product species are identified and found to be at least 9 Å away from each other. The expressions used to determine the reaction attributes and the sampling scheme are given in Refs. 3 and 4.

Thermal Rate Constants

Experimental determinations of the thermal rate constants of reaction (2) have only been made up to the moderately high temperature of 3000 K.[1] Moreover, these rates are often associated with uncertainties because of interference from reaction (1), which is difficult to separate at temperatures above 2000 K. The most widely used rate expression is $6.4 \times 10^9 T \exp(-3150/T)$ cm^3 mol^{-1} s^{-1} recommended by Baulch et al.[1] For high-temperature flow calculations, Park et al.[16] recommend $8.4 \times 10^{12} \exp(-19450/T)$ cm^3 mol^{-1} s^{-1} for the backward reaction (NO + O → O_2 + N), which is used with the detailed balance principle to compute the rate of reaction (2). In practice, these rates are extrapolated to high temperatures for hypersonic flow simulations.

Figure 1 plots the QCT-based rate of reaction (2), along with the expressions based on experimental data. As can be seen, good agreement is obtained with the recommended data, except for the expression of Park et al.,[16] which was obtained by fitting the experimental data on the backward reaction between 2000 and 5000 K, where there is reasonably good agreement. However, the temperature dependence predicted by the expression of Park et al. strongly disagrees with all other recommendations; at temperatures above 10,000 K the difference is almost an order of magnitude. Thus, using the QCT rates in flow simulation codes may result in a significant increase in NO formation.

The following modified Arrhenius rate expression is obtained using the QCT data

$$k(T) = 2.49 \times 10^9 T^{1.179} \exp(-4005.5/T) \quad \text{cm}^3\ \text{mol}^{-1}\ \text{s}^{-1} \tag{3}$$

for $1000 \le T \le 14{,}000$ K. Because this expression is obtained with a least-squares fit, the parameters must be viewed as simply an outcome of the fit.

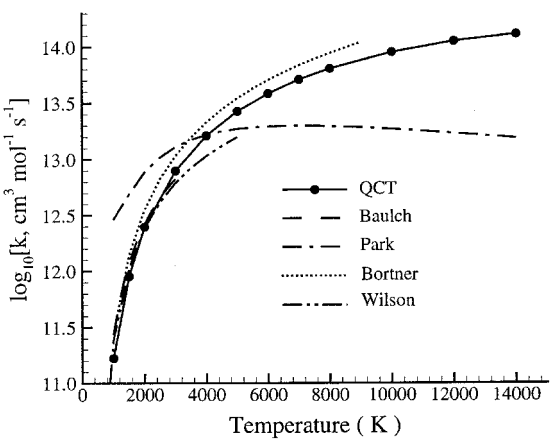

Fig. 1 Comparison of the rate constant of reaction (2) obtained in this work with various recommended data based on experiments listed in Ref. 1.

Rate Constants for Nonequilibrium Flows

Because hypersonic flows are generally characterized by multiple temperatures, a thermally averaged reaction rate is of limited use. The rate constant must be available as a function of the translational T_t, rotational T_r, and vibrational T_v temperatures of the reactants. In this section we use the QCT method to predict the effect of thermal nonequilibrium on the rate of reaction (2). To make comparisons, we also present similar data for reaction (1) obtained previously.[2–5]

Let us consider the variation of the thermal rate constant of reaction (2) with respect to the reactant (O_2) vibrational temperature. This is obtained by sampling the vibrational energy of O_2 molecules from a Boltzmann distribution at T_v. The nonequilibrium rate data are plotted in Fig. 2a for various translational–rotational temperatures T. It is seen that there is a relatively mild effect of vibrational nonequilibrium on the rate of reaction (2). This is expected because this reaction is exothermic and the reaction path has an early barrier. When T_v is decreased from T to 1000 K, the rate is reduced from its equilibrium value by only a factor of 1.09 at T = 3000 K, and a factor of 1.3 at T = 14,000 K. This is a much smaller effect than obtained for reaction (1), as shown in Fig. 2b. The value of reactant T_r causes an even smaller effect on the rate of reaction (2). Thus, for convenience we neglect the influence of T_r on the reaction rate and assume $T_r = T_t = T$ for the QCT calculations. When $T_r \neq T_t$, we assume $T = T_t$ and safely ignore the value of T_r, for the purpose of computational fluid dynamics (CFD) modeling. Thus, in a CFD simulation, rotational nonequilibrium is still important to obtain an accurate value of T_r.

The rate constant of reaction (2) as a function of T and T_v

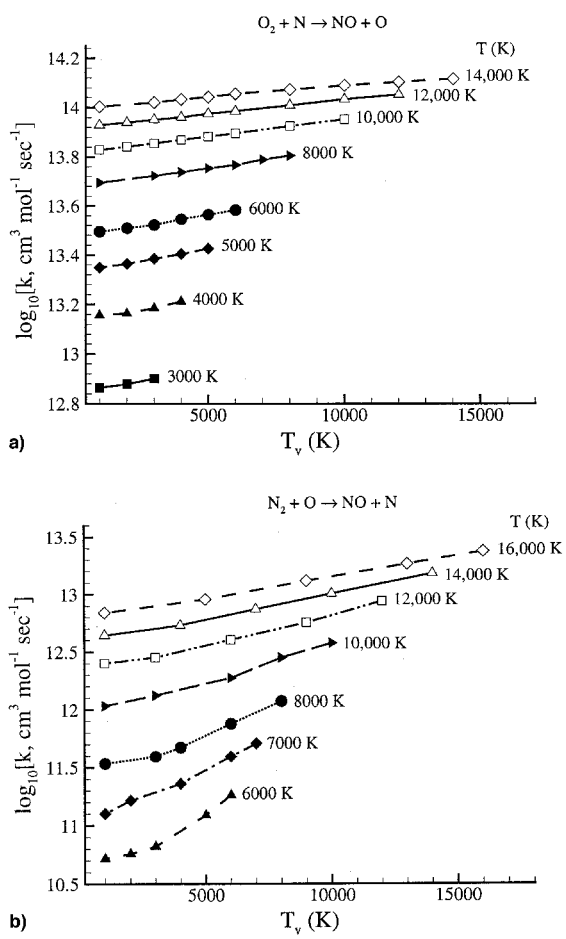

Fig. 2 Thermal nonequilibrium rate constants of the Zeldovich reactions: a) (2) and b) (1).

is represented analytically by fitting the QCT data. We use a total of 51 data points in the range

$$T = 3000\text{–}14{,}000 \text{ K}$$
$$T_v = 1000\text{–}14{,}000 \text{ K} \tag{4}$$

for $T_v \leq T$. The reaction rate is expressed as

$$k(T, T_v) = \exp\left(\sum_{i,j} a_{ij} T^i T_v^j\right) \quad \text{cm}^3 \text{ mol}^{-1} \text{ s}^{-1} \tag{5}$$

where the temperatures are in K and the coefficients a_{ij} are obtained using a least-squares algorithm, and are given in Table 1. A similar expression for the rate constant for reaction (1) was obtained in Ref. 5.

Energy Removal and Disposal Modeling

In this section we discuss the energy removal and disposal of reaction (2) under thermal nonequilibrium conditions.

Table 1 Coefficients of the polynomial fit [Eq. (5)] describing the effect of vibrational nonequilibrium on the rate constant of reaction (2)

a_{00}	$2.710 \times 10^{+01}$	a_{11}	-5.867×10^{-09}
a_{01}	5.384×10^{-05}	a_{10}	1.073×10^{-03}
a_{02}	3.413×10^{-09}	a_{20}	-8.338×10^{-08}
a_{03}	-2.122×10^{-14}	a_{30}	2.349×10^{-12}
a_{12}	-2.484×10^{-13}	a_{21}	2.759×10^{-13}
ΔE_{rms}	0.012	ΔE_{max}	0.028

Again, we present the same information for reaction (1) for comparison purposes.

The fact that the vibrational temperature of O_2 only marginally affects the rate of reaction (2) implies that there should be little preferential removal of O_2 as a result of reaction (2). This is shown in Fig. 3a, which presents the average vibrational energy of O_2 removed per reactive collision vs the reactant T_v at various translational–rotational temperatures. The solid line represents the average reactant vibrational energy at T_v. This shows that the average O_2 vibrational energy removed per reactive collision is close to the average O_2 vibrational energy and there is little preferential removal. This is quite different than reaction (1), as shown in Fig. 3b.

Let us now discuss the vibrational energy of the NO formed by reaction (2). As can be seen in Fig. 4a, the NO molecules are formed with a much higher vibrational energy than that of an average NO molecule at the reactant T_v. This is primarily because of the exothermicity of reaction (2) and a preferential channeling of the reactant translational energy into product vibration. It is also found that the product NO vibrational energy increases rapidly with increasing reactant vibrational temperature. This is because the O_2 vibrational level strongly determines the NO vibrational energy disposal, as noted in Ref. 9. On the other hand, the NO molecules formed by reaction (1) are vibrationally hotter than the reactant N_2 only when T_v is much lower than T. Under near-equilibrium conditions, the product NO vibrational energy is close to the average reactant vibrational energy. In summary, the NO formed by reaction (2) is always on average vibrationally hot, while that produced by reaction (1) is only vibrationally hot when the reactant vibrational temperature is lower than the translational–rotational

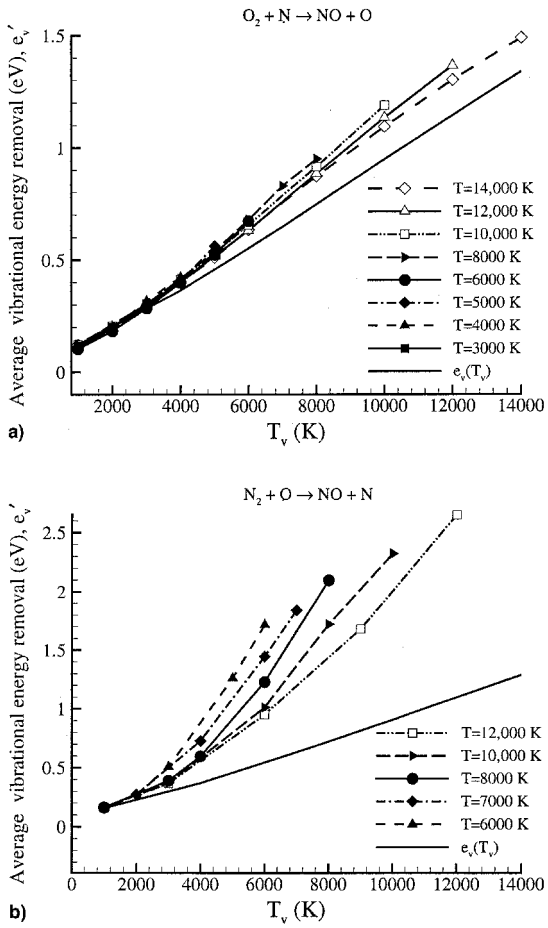

Fig. 3 Variation of reactant vibrational energy removal with T_v at various translational–rotational temperatures: a) reaction (2) and b) reaction (1). ——, average vibrational energy of the reactant molecule at T_v.

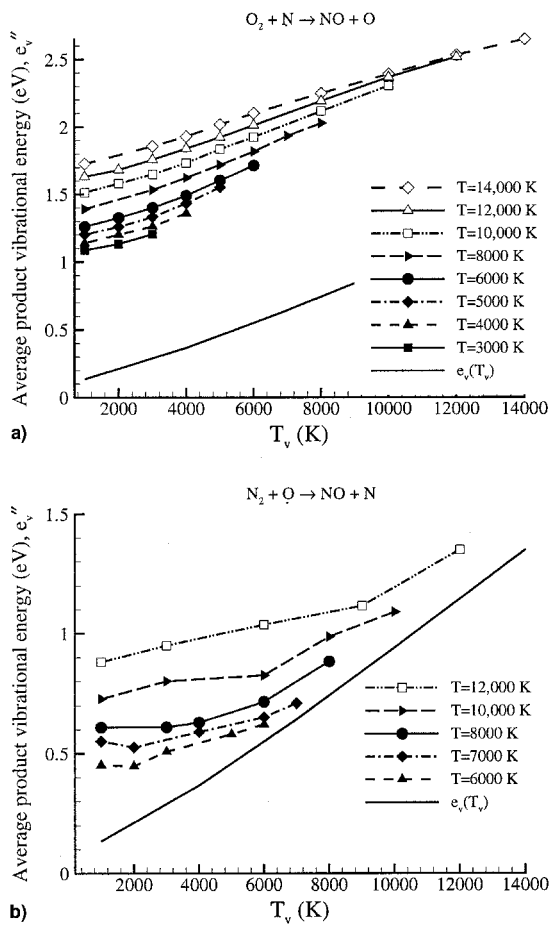

Fig. 4 Variation of product NO vibrational energy with reactant T_v at various translational–rotational temperatures: a) reaction (2) and b) reaction (1). ——, average NO vibrational energy at T_v.

Table 2 Coefficients of the polynomial fit [Eq. (8)] describing the reactant vibrational energy removal and product vibrational energy disposal because of reaction (2)

	e'_v	e''_v
a_{00}	5.714×10^{-08}	8.194×10^{-01}
a_{01}	8.715×10^{-05}	3.581×10^{-05}
a_{02}	5.470×10^{-09}	9.260×10^{-09}
a_{03}	-2.838×10^{-13}	-2.138×10^{-13}
a_{10}	$0.000 \times 10^{+00}$	6.558×10^{-05}
a_{11}	$0.000 \times 10^{+00}$	2.443×10^{-09}
a_{12}	$0.000 \times 10^{+00}$	-3.639×10^{-13}
a_{20}	$0.000 \times 10^{+00}$	1.094×10^{-10}
a_{21}	$0.000 \times 10^{+00}$	-8.780×10^{-14}
a_{30}	$0.000 \times 10^{+00}$	-3.222×10^{-14}
ΔE_{rms}	0.022	0.008
ΔE_{max}	0.054	0.020

temperature. The implications of this effect in hypersonic flows will be discussed in the next section.

Let e'_v be the O_2 vibrational energy removed from the reactants per reactive collision, and e''_v be the NO vibrational energy disposed to the products by reaction (2). We fit these two quantities using the QCT data with the following expression:

$$e'_v = \sum_{i,j} a_{ij} T^i T_v^j \quad \text{eV} \tag{6}$$

and likewise for e''_v. The values of a_{ij} are given in Table 2; similar expressions for reaction (1) were obtained in Ref. 5.

Hypersonic Flow Computations

In this section we study the implications of our QCT study in several hypersonic flowfields. In addition to reactions (1) and (2), three dissociation reactions are modeled

$$\begin{aligned} N_2 + M &\rightleftharpoons N + N + M, \qquad (9.76\ \text{eV}) \\ O_2 + M &\rightleftharpoons O + O + M, \qquad (5.12\ \text{eV}) \\ NO + M &\rightleftharpoons N + O + M, \qquad (6.49\ \text{eV}) \end{aligned} \tag{7}$$

where M is a collision partner. We use CFD to solve conservation equations for the following flow variables: species density ρ_s, total gas momentum per unit volume in the x and y direction ρu and ρv, vibrational and rotational energy of NO per unit volume $E_{v,\text{NO}}$ and $E_{r,\text{NO}}$, combined vibrational and rotational energy of N_2 and O_2 per unit volume $E_{v,g}$ and $E_{r,g}$, and total energy unit volume E. This forms a set of 12 simultaneous equations that may be written in conservation-law form as

$$\frac{\partial \boldsymbol{U}}{\partial t} + \frac{\partial (\boldsymbol{F}_I + \boldsymbol{F}_V)}{\partial x} + \frac{\partial (\boldsymbol{G}_I + \boldsymbol{G}_V)}{\partial y} = \boldsymbol{W} \tag{8}$$

where $\boldsymbol{U}$ is the vector of conserved quantities, $\boldsymbol{F}_I$ and $\boldsymbol{G}_I$ are the convective flux vectors in the x and y directions, $\boldsymbol{F}_V$ and $\boldsymbol{G}_V$ are the diffusive flux vectors, and $\boldsymbol{W}$ is the source vector as a result of chemical reactions and energy exchange. Consider the internal energy equations of NO and N_2, O_2; the relevant portions of the vectors are

$$\boldsymbol{U} = \begin{pmatrix} E_{v,\text{NO}} \\ E_{r,\text{NO}} \\ E_{v,g} \\ E_{r,g} \end{pmatrix}, \qquad \boldsymbol{F}_I = \begin{pmatrix} E_{v,\text{NO}} u \\ E_{r,\text{NO}} u \\ E_{v,g} u \\ E_{r,g} u \end{pmatrix} \tag{9}$$

$$\boldsymbol{F}_V = -\begin{bmatrix} \rho e_{v,\text{NO}} \mathcal{D}_{\text{NO}} \dfrac{\partial c_{\text{NO}}}{\partial x} + \kappa_{v,\text{NO}} \dfrac{\partial T_{v,\text{NO}}}{\partial x} \\ \rho e_{r,\text{NO}} \mathcal{D}_{\text{NO}} \dfrac{\partial c_{\text{NO}}}{\partial x} + \kappa_{r,\text{NO}} \dfrac{\partial T_{r,\text{NO}}}{\partial x} \\ \rho e_{v,\text{N}_2} \mathcal{D}_{\text{N}_2} \dfrac{\partial c_{\text{N}_2}}{\partial x} + \rho e_{v,\text{O}_2} \mathcal{D}_{\text{O}_2} \dfrac{\partial c_{\text{O}_2}}{\partial x} + \kappa_{v,g} \dfrac{\partial T_{v,g}}{\partial x} \\ \rho e_{r,\text{N}_2} \mathcal{D}_{\text{N}_2} \dfrac{\partial c_{\text{N}_2}}{\partial x} + \rho e_{r,\text{O}_2} \mathcal{D}_{\text{O}_2} \dfrac{\partial c_{\text{O}_2}}{\partial x} + \kappa_{r,g} \dfrac{\partial T_{r,g}}{\partial x} \end{bmatrix} \tag{10}$$

where $e_{v,s}$ and $e_{r,s}$ are defined to be $E_{v,s}/\rho$ and $E_{r,s}/\rho$, respectively, $\mathcal{D}_s$ is the diffusion coefficient, and c_s is the mass fraction of species s. $\kappa_{v,s}$ and $\kappa_{r,s}$ are the vibrational and rotational heat conductivities. The temperature, $T_{v,\text{NO}}$, characterizes the vibrational energy of NO and $T_{v,g}$ characterizes the combined N_2, O_2 vibrational energy. We define $T_{r,\text{NO}}$ and $T_{r,g}$ similarly.

The source vector is written as

$$\boldsymbol{W} = \begin{pmatrix} Q_{v,\text{NO}}[\text{exch}] + Q_{v,\text{NO}}[\text{chem}] \\ Q_{r,\text{NO}}[\text{exch}] + Q_{r,\text{NO}}[\text{chem}] \\ Q_{v,\text{N}_2}[\text{exch}] + Q_{v,\text{N}_2}[\text{chem}] + Q_{v,\text{O}_2}[\text{exch}] + Q_{v,\text{O}_2}[\text{chem}] \\ Q_{r,\text{N}_2}[\text{exch}] + Q_{r,\text{N}_2}[\text{chem}] + Q_{r,\text{O}_2}[\text{exch}] + Q_{r,\text{O}_2}[\text{chem}] \end{pmatrix} \tag{11}$$

The quantities $Q_{v,s}[\text{exch}]$ and $Q_{r,s}[\text{exch}]$ represent the rate of energy exchange per unit volume as a result of nonreactive collisions in the flowfield. This includes vibration–translation (VT), vibration–vibration (VV), rotation–translation (RT), and rotation–rotation (RR) energy transfers. We use the first-order perturbation expression developed for VT relaxation by Landau and Teller[17] with semiempirical relaxation times of Millikan and White.[18] For VV transfer we use the first-order perturbation expression of Schwartz et al.[19] with a transition probability, P^{1-0}_{0-1}, of 0.01. The RT transfer is predicted by the classical model of Parker.[20] Because of a lack of appropriate models, we use an RR relaxation time of 10 collision times, which is expected to be close to the actual value.

The quantities $Q_{v,s}[\text{chem}]$ and $Q_{r,s}[\text{chem}]$ in $\boldsymbol{W}$ represent the rate of energy redistribution per unit volume because of the chemical reactions; data for these energy transfer rates are obtained from the QCT-based fits.

In this paper we simulate the BSUV1 and BSUV2 flight experiments to compare the results of the new models with experimental data. These experiments made spectrally resolved measurements of the uv emission in the stagnation region of the vehicle. The first flight flew at a speed of 3.5 km/s, and took measurements from 37 to 75 km altitude. The second flight flew at 5.11 km/s and made measurements during reentry from 90 to 65 km altitude. Both vehicles consisted of a 4 in. (10.16 cm) nose radius spherically blunted cone. The experimental spectra are found to be dominated by the NO γ and β systems because of the NO(A $\rightarrow X$) and NO(B $\rightarrow X$) transitions.

It was concluded by Levin et al.[7,8] and Boyd et al.[21] that previous state-of-the-art flow simulation and radiation modeling methods could only match the experimental spectral radiance within about two orders of magnitude at high altitudes. Also, the predicted relative peak intensities of different transitions did not match the spectrometer data. The flow simulation code used for those simulations employed the Park $\sqrt{TT_v}$ model[22] for vibration–dissociation coupling and the rates recommended by Park et al.[16] for the Zeldovich reactions. The effects of thermal nonequilibrium on the rates of the Zeldovich reactions were neglected. Also, it was assumed that NO was formed with a vibrational energy equal to the average gas vibrational energy. Moreover, only one vibrational temperature was used to characterize the three diatomic species. In this paper we consider this as the baseline model.

In this work we use the QCT data to improve the NO kinetics models. First, we employ the Macheret and Rich[23] vibration–dissociation coupling model for the N_2 and O_2 thermal nonequilibrium dissociation rates. This model was shown by Boyd et al.[21] to improve the NO concentration predictions by increasing the O_2 dissociation rate under strong nonequilibrium conditions. We also solve separate conservation equations for the vibrational and rotational energies of NO. This is referred to as model I. The Zeldovich reactions are treated in the same manner as in the baseline model.

Model II includes the improvements employed in model I, and we use the QCT data to model the first Zeldovich reaction. This is done by using the thermal nonequilibrium rate constant, energy removal, and energy disposal expressions from Ref. 5.

Model III extends model II by using the current QCT data to model the second Zeldovich reaction. Table 3 summarizes the different models discussed.

Table 3 Various models used to treat the Zeldovich reactions in the CFD code

	$N_2 + O \rightarrow NO + N$	$O_2 + N \rightarrow NO + O$
Model I	Rate: Park et al.[22]	Rate: Park et al.[22]
	NO energy disposal: Average energy	NO energy disposal: Average energy
Model II	Rate: QCT (Ref. 5)	Rate: Park et al.[22]
	NO energy disposal: QCT (Ref. 5)	NO energy disposal: Average energy
Model III	Rate: QCT (Ref. 5)	Rate: QCT [Eq. (5)]
	NO energy disposal: QCT (Ref. 5)	NO energy disposal: QCT [Eq. (6)]

Results and Discussion

BSUV1 Flows

Let us first consider the effect of modeling enhancements on the amount of NO formed at the BSUV1 flight conditions. Figure 5 plots the NO mass fraction profiles along the stagnation streamline at 53.5 and 63 km altitudes. Model I produces more NO than the baseline model because the Macheret and Rich vibration-dissociation coupling model[23] predicts higher O_2 dissociation rates than the Park model[24] when $T_v << T$. Increased formation of atomic oxygen results in more NO formation via reaction (1). The NO mass fraction predicted by model I is more than an order of magnitude higher than that predicted by the baseline model at a location 1 cm away from the body surface; this is where T_t and the radiative emission reach their maximum levels.

When we use model II, the NO concentration decreases in the flowfield compared with using model I. This is because of the reduction of the rate of reaction (1) by vibrational nonequilibrium. The relative difference between the predictions of the NO mass fraction by models I and II increases with altitude due to stronger vibrational nonequilibrium. Model III produces almost no change in the NO mass fraction because at BSUV1 conditions, the QCT and Park et al.[16] rate expressions for reaction (2) are similar (Fig. 1).

The models produce significantly different NO vibrational temperatures along the stagnation streamline, as seen in Fig. 6. As mentioned earlier, the baseline model does not solve for a separate vibrational temperature of NO, thus, in that model $T_{v,NO}$ is equal to $T_{v,g}$. In model I a separate vibrational energy equation is solved, but because NO is assumed to be formed with the average vibrational energy, $T_{v,NO}$ is very close to $T_{v,g}$. The small difference near the shock is caused by the diffusion of high-energy NO molecules across the bow shock wave.

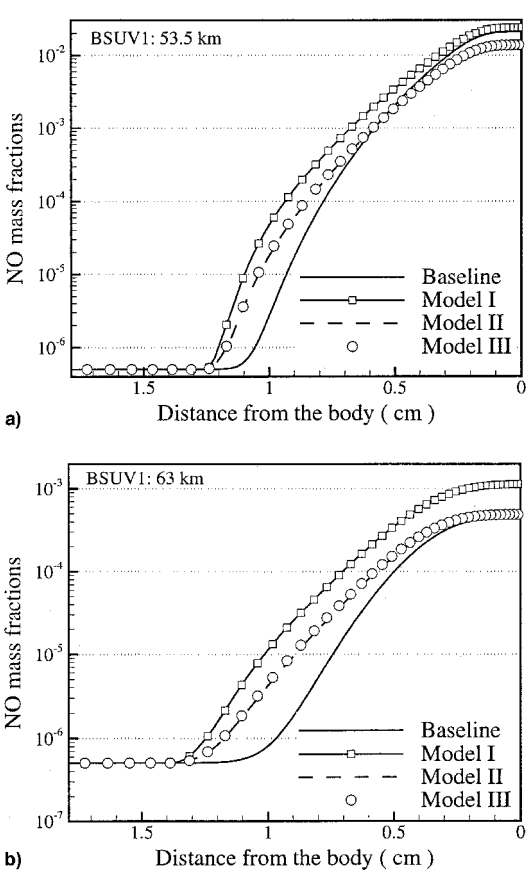

Fig. 5 Computed stagnation streamline mass fractions for BSUV1: a) 53.5 and b) 63 km.

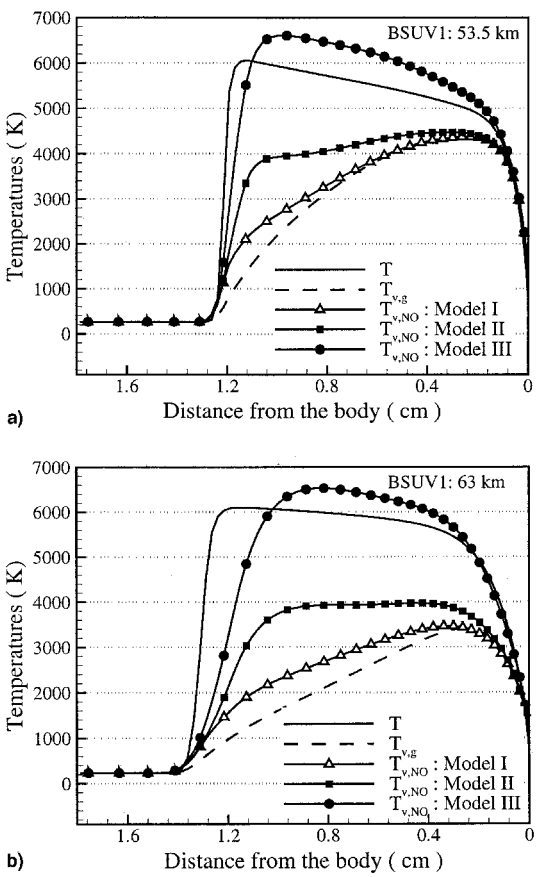

Fig. 6 Computed stagnation streamline temperature profiles for BSUV1 (T and $T_{v,g}$ are plotted only once because they are extremely close for all models): a) 53.5 and b) 63 km.

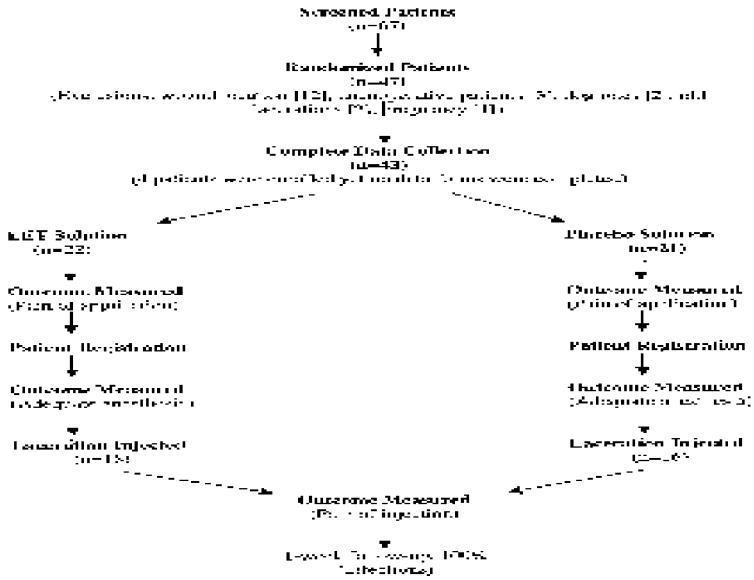

Fig. 7 Computed and BSUV1 experimental stagnation line spectra at 53.5 km altitude.

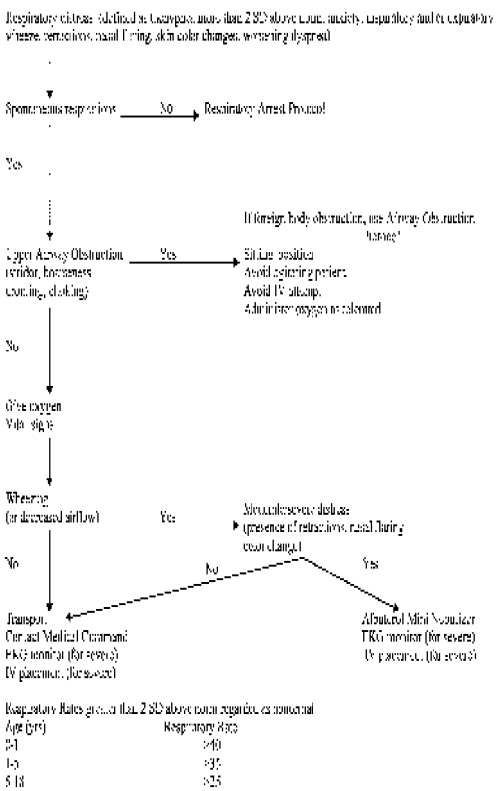

Fig. 8 Computed stagnation streamline mass fractions for BSUV2: a) 79 and b) 85 km.

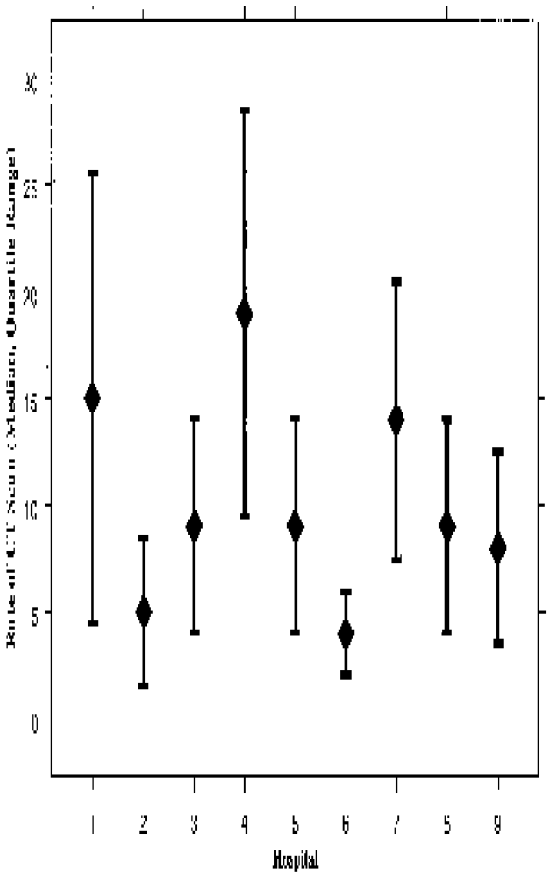

Fig. 9 Computed stagnation streamline temperature profiles for BSUV2 (T_r and $T_{v,g}$ are plotted only once because they are extremely close for all models): a) 79 and b) 85 km.

When we use the QCT-based model for energy disposal resulting from reaction (1), there is an increase of $T_{v,\mathrm{NO}}$ because of the vibrationally hot NO formation via reaction (1). The biggest difference in $T_{v,\mathrm{NO}}$ is caused by model III, which adds the QCT-based model for reaction (2). This reaction forms about 30% of the NO molecules in the stagnation region. Because a large fraction of the reaction exothermicity is channeled into product vibrational energy, $T_{v,\mathrm{NO}}$ is very large in these flows. The fact that $T_{v,\mathrm{NO}}$ is higher than T is not surprising because the high $T_{v,\mathrm{NO}}$ is caused by energy disposal, and not by energy relaxation.

The results of these flowfield calculations were used as input to the nonequilibrium air radiation (NEQAIR) code,[24,25] and the stagnation line spectra were computed. For the purposes of this discussion, the radiation modeling is assumed to be correct. Figure 7 compares the experimental and predicted uv spectral radiance in the 200–250 nm range. We have normalized the predicted spectra relative to the data at 226 nm to make the comparison of the spectral features possible. The magnitude of the spectra depends only on the number of NO molecules, and not on the internal energy modeling. The baseline model and models I and II predict the relative peak heights well, except for the peak at 204 nm. However, the most de-

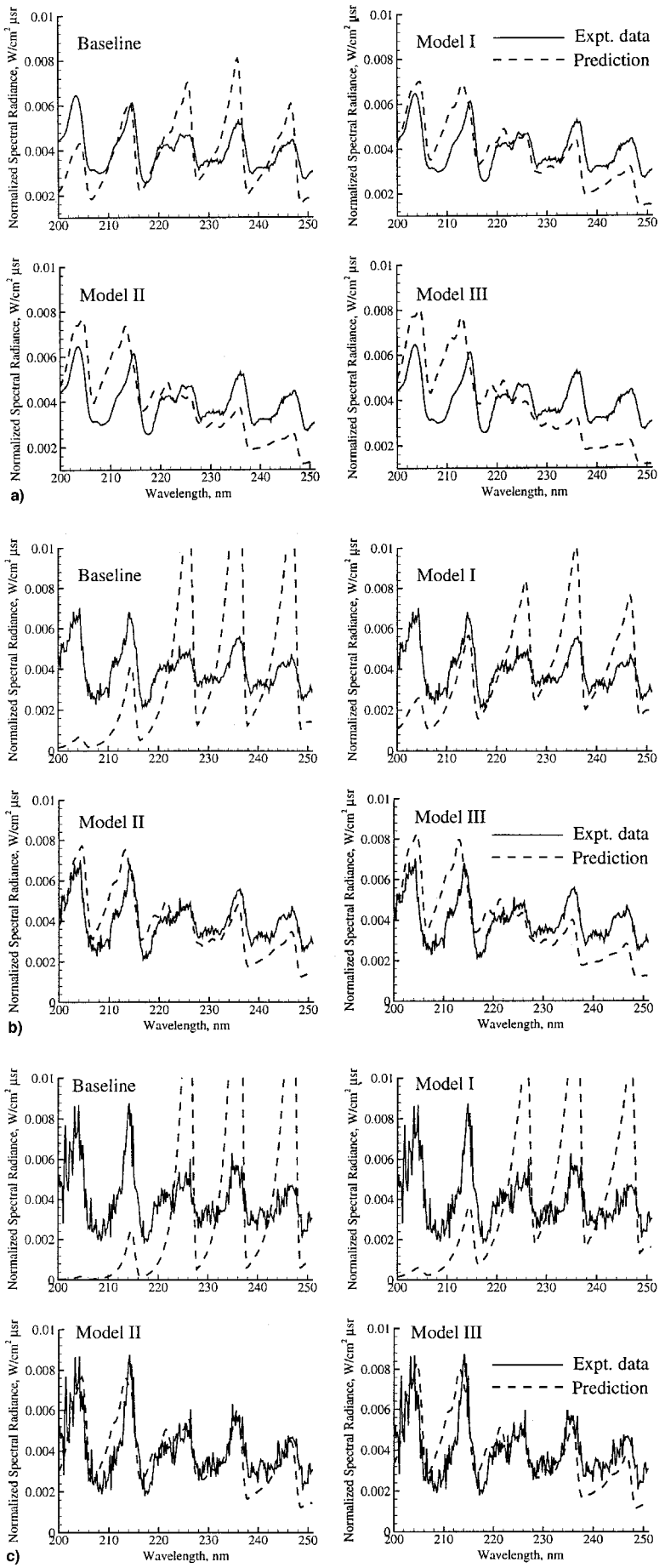

Fig. 10 Computed and BSUV2 experimental stagnation line spectra at: a) 79, b) 85, and c) 87.5 km altitudes.

tailed model (model III) gives relatively poor agreement, which is indicative of an overly high vibrational temperature. Thus, it appears that the high vibrational temperatures predicted by model III are spurious, and it is likely that there are other mechanisms that cool the vibrational temperature of NO. A possible mechanism is an NO destruction reaction that selectively consumes the high vibrational energy NO molecules, resulting in lower $T_{v,NO}$. Another possibility is a more rapid VV draining of the NO vibrational energy. Because these effects depend on the collision rate, they must become less important in rarefied flows; this will be further discussed for the BSUV2 flows.

BSUV2 Flows

Figure 8 plots the NO mass fraction profiles predicted by the different models. At 79 km there is not much difference between the various NO mass fractions obtained. The lowest NO production is with the baseline model, as a result of the use of the $\sqrt{TT_v}$ model. Large differences occur at 85 km, where an increase in the NO mass fraction occurs as a result of the improved vibration–dissociation coupling model (model I). The NO mass fraction decreases when model II is used because of the reduction of the rate of reaction (1) by thermal nonequilibrium. Model III increases the NO mass fraction because the QCT-based rate of reaction (2) is about an order of magnitude larger than the Park rate[24] at these conditions. However, because reaction (2) forms only about 12% of the NO, its effect on the overall NO mass fraction is fairly small.

Figure 9 shows the $T_{v,NO}$ predicted by the different models at 79 and 85 km. It is seen that model I predicts a higher NO vibrational temperature than $T_{v,g}$, although NO is assumed to form at the average vibrational energy of the gas. This appears surprising at first; however, there are several reasons for this effect. First, the VT rates for NO are higher than for N_2 and O_2, causing $T_{v,NO}$ to rise faster. Secondly, as observed in the BSUV1 flows, the increase of $T_{v,NO}$ near and upstream of the shock is caused by the upstream diffusion of high-energy NO molecules from inside the shock layer. Models II and III increase $T_{v,NO}$ because of the use of the QCT-based energy disposal modeling. At 85 km and higher, reaction (2) is not a significant contributor to NO formation, and model III has a small effect.

Figure 10 plots the computed normalized spectra at 79, 85, and 87.5 km altitude predicted by the different models. Model I improves the predictions of the uv spectra because of the increased $T_{v,NO}$. However, there remains poor agreement of the relative peak heights at 85 and 87.5 km. The QCT-based energy disposal models (models II and III) produce better agreement with the experimental spectra. This is the most significant result of this analysis, as it is a direct test of the NO vibrational energy disposal model used in the flow simulation. Because of the rarefied nature of these flows, the product NO vibrational temperature remains unperturbed by the other collision-based mechanisms. The slight worsening of the agreement with models II and III at 79 km is again likely caused by these mechanisms that rapidly lower $T_{v,NO}$ by removing highly excited NO molecules.

Conclusions

Thermally averaged QCT rates are presented for the second Zeldovich reaction, $O_2 + N \rightarrow NO + O$, based ab initio potential energy surfaces. The thermal equilibrium rate constants are found to be in good agreement with various experimental and recommended data, with the exception of the rates derived from the expression recommended by Park et al.[17] For this reaction, the vibrational temperature of the reactants has a limited effect on the reaction rate. The average NO vibrational energy of the molecules formed by this reaction is much higher than the reactant O_2 vibrational energy because the reaction exothermicity is channeled into the products. The QCT database is used to develop a flowfield model for high-temperature nonequilibrium airflows. CFD is used to simulate two recent flight experiments. The detailed model for the second Zeldovich reaction does not appreciably alter the NO mass fractions; however, it significantly raises the NO vibrational temperature. At high altitudes, this higher NO vibrational temperature produces better agreement with the radiation data; however, at low altitudes, the agreement worsens. This is most likely a result of additional collisional processes that quickly remove the highly excited NO molecules. Therefore, to further improve the agreement, these processes must be included in the flowfield model.

Acknowledgments

Support for the authors is provided by the U.S. Army Research Office under Grant DAAH04-93-G-0089. This work was also sponsored in part by the U.S. Army High Performance Computing Research Center under the auspices of the Department of the Army, Army Research Laboratory cooperative agreement number DAAH04-95-2-0003/Contract DAAH04-95-C-0008, the content of which does not necessarily reflect the position or the policy of the government, and no official endorsement should be inferred. We would like to thank Jim W. Duff for providing us with his analytical PES parameters. We are also indebted to Deborah A. Levin for help in computing the spectra.

References

[1]Baulch, D. L., Drysdale, D. D., and Haine, D. G., *Evaluated Kinetic Data for High Temperature Reactions*, Butterworths, London, 1973.

[2]Bose, D., and Candler, G. V., "Thermal Rate Constants of the $N_2 + O \rightarrow NO + N$ Reaction Using *Ab Initio* $^3A''$ and $^3A'$ Potential Energy Surfaces," *Journal of Chemical Physics*, Vol. 104, No. 8, 1996, pp. 2825–2833.

[3]Bose, D., and Candler, G. V., "Kinetics of the $N_2 + O \rightarrow NO + N$ Reaction Under Thermodynamic Nonequilibrium," *Journal of Thermophysics and Heat Transfer*, Vol. 10, No. 1, 1996, pp. 148–154.

[4]Bose, D., and Candler, G. V., "Kinetics of the $N_2 + O \rightarrow NO + N$ Reaction in Nonequilibrium Flows," AIAA Paper 96-0104, Jan. 1996.

[5]Bose, D., and Candler, G. V., "Simulation of Hypersonic Flows Using a Detailed Nitric Oxide Formation Model," *Physics of Fluids*, Vol. 9, No. 4, 1997, pp. 1171–1181.

[6]Boyd, I. D., Bose, D., and Candler, G. V., "Development of a Monte Carlo Chemistry Model Based on Quasi-Classical Trajectory Calculations," *Physics of Fluids*, Vol. 9, No. 4, 1997, pp. 1162–1170.

[7]Levin, D. A., Candler, G. V., Collins, R. J., Erdman, P. W., Zipf, E. C., and Howlett, C., "Examination of Theory for Bow Shock Ultraviolet Rocket Experiments—I," *Journal of Thermophysics and Heat Transfer*, Vol. 8, No. 3, 1994, pp. 447–452.

[8]Levin, D. A., Braunstein, M., Candler, G. V., Collins, R. J., and Smith, G., "Examination of Theory for Bow Shock Ultraviolet Rocket Experiments—II," *Journal of Thermophysics and Heat Transfer*, Vol. 8, No. 3, 1994, pp. 453–459.

[9]Bose, D., and Candler, G. V., "Thermal Rate Constants of the $O_2 + N \rightarrow NO + O$ Reaction Based on the $^2A'$ and $^4A'$ Potential Energy Surfaces," *Journal of Chemical Physics*, Vol. 107, No. 16, 1997, pp. 6136–6145.

[10]Sharma, R. D., Sun, Y., and Dalgarno, A., "Highly Rotationally Excited Nitric Oxide in the Terrestrial Thermosphere," *Geophysical Research Letters*, Vol. 20, No. 19, 1993, pp. 2043–2045.

[11]Duff, J. W., Bien, F., and Paulsen, D. E., "Classical Dynamics of the $N(^4S_u) + O_2(X\,^3\Sigma_g^-) \rightarrow NO(X\,^2\Pi) + O(^3P_g)$," *Geophysical Research Letters*, Vol. 21, No. 18, 1994, pp. 2043–2046.

[12]Gilibert, M., Aguilar, A., González, M., Mota, F., and Sayós, R., "Dynamics of the $N(^4S_u) + NO(X\,^2\Pi) \rightarrow N_2(X\,^1\Sigma_g^+) + O(^3P_g)$ Atmospheric Reaction on the $^3A''$ Ground Potential Energy Surface. I. Analytical Potential Energy Surface and Preliminary Quasiclassical Trajectory Calculations," *Journal of Chemical Physics*, Vol. 97, No. 8, 1992, pp. 5542–5553.

[13]Walch, S. P., and Jaffe, R. L., "Calculated Potential Surfaces for the Reactions: $O + N_2 \rightarrow NO + N$ and $N + O_2 \rightarrow NO + O$," *Journal of Chemical Physics*, Vol. 86, No. 12, 1987, pp. 6946–6956.

[14]Walch, S. P., and Jaffe, R. L., American Inst. of Physics Document PAPS JCPSA-86-6946-10.

[15]Truhlar, D. G., and Muckerman, J. T., "Reactive Scattering Cross Sections III: Quasiclassical and Semiclassical Methods," *Atom Molecule Collision Theory*, edited by R. B. Bernstein, Plenum, New York, 1979, pp. 505–561.

[16]Park, C., Howe, J. T., Jaffe, R. L., and Candler, G. V., "Review of Chemical-Kinetic Problems of Future NASA Missions, II: Mars Entries," *Journal of Thermophysics and Heat Transfer*, Vol. 8, No. 1, 1994, pp. 9–23.

[17]Landau, L., and Teller, E., "Theory of Sound Dispersion," *Physikalische Zeitschrift der Sowjetunion*, Vol. 10, No. 1, 1936, p. 34.

[18]Millikan, R. C., and White, D. R., "Systematics of Vibrational Relaxation," *Journal of Chemical Physics*, Vol. 39, No. 1, 1963, pp. 98–101.

[19]Schwartz, R. N., Slawsky, Z. I., and Herzfeld, K. F., "Calculation of Vibrational Relaxation Times in Gases," *Journal of Chemical Physics*, Vol. 20, No. 10, 1952, pp. 1591–1599.

[20]Parker, J. G., "Rotational and Vibrational Relaxation in Diatomic Gases," *Physics of Fluids*, Vol. 2, No. 4, 1959, pp. 449–462.

[21]Boyd, I. D., Candler, G. V., and Levin, D. A., "Dissociation Modeling in Low Density Hypersonic Flows of Air," *Physics of Fluids*, Vol. 7, No. 7, 1995, pp. 1757–1763.

[22]Park, C., "Assessment of a Two Temperature Kinetic Model for Dissociating and Weakly Ionizing Nitrogen," *Journal of Thermophysics and Heat Transfer*, Vol. 2, No. 1, 1988, pp. 8–16.

[23]Macheret, S. O., and Rich, J. W., "Nonequilibrium Dissociation Rates Behind Strong Shock Waves: Classical Model," *Chemical Physics*, Vol. 174, 1993, pp. 25–43.

[24]Park, C., "Calculation of Nonequilibrium Radiation in the Flight Regimes of Aeroassisted Orbital Transfer Vehicles," *Thermal Design of Aeroassisted Orbital Transfer Vehicles*, edited by H. F. Nelson, Vol. 96, Progress in Aeronautics and Astronautics, New York, 1985, pp. 395–418.

[25]Laux, C. O., Gessman, R. J., and Kruger, C. H., "Modeling the UV and VUV Radiative Emission of High-Temperature Air," AIAA Paper 93-2802, July 1993.